Modeling of a New Torque Controller for Direct Torque Control of Induction Machines

Nik Rumzi Nik Idris
E-mail: nikrumzi@ieee.org

Abdul Halim Mohd Yatim
E-mail: halim@ieee.org

Department of Energy Conversion,
Faculty of Electrical Engineering,
Universiti Teknologi Malaysia,
81310 UTM Skudai, Johor,
MALAYSIA
http://suria.fke.utm.my/~tenaga

Abstract: In this paper a new torque controller for Direct Torque Control (DTC) of induction motor drives is proposed. The structure of the new controller is very simple with its output similar to that of the conventional three level hysteresis comparator. The approximate frequency domain model of the proposed controller is presented which served as a guide for the selection of the controller's parameters. The simulation of the DTC of IM with the proposed torque controller is presented which is verified by experimental results. The results indicate that the proposed controller is capable of maintaining the torque switching frequency constant and reducing the torque ripple, particularly at low speed.

I. INTRODUCTION

In its basic configuration, a DTC drive, shown in Fig. 1, consists of a pair of hysteresis comparators, torque and flux estimator, voltage vector selector and a Voltage Source Inverter (VSI) [1]. Despite its simplicity, DTC drives offer comparable or even better torque performance than that of DC machines and FOC drives. The torque and stator flux are regulated within their hysteresis bands independently by applying appropriate voltage vectors to the VSI. The voltage vectors are selected based on the outputs of the torque and stator flux hysteresis comparators as well as the stator flux orientation.

It is shown in [2,3,4], that the rate of change of torque and stator flux and hence the time taken for the flux and torque to touch their upper and lower bands depend on the operating conditions, i.e. rotor speed, stator and rotor fluxes and DC link voltage. Since the device switching frequency of the VSI, is directly related to the switching of the torque and stator flux hysteresis comparators, it follows that the device switching frequency depends on the operating conditions. Variable switching frequency resulted in an unpredictable harmonic current flow. The maximum capability of the inverter is not fully utilized. For fixed torque band, the choice of the hysteresis band's width is normally based on the worst case condition which is limited by the thermal condition of the switching devices, thus operation in other conditions are not optimized. At low speed, the positive torque slope is large which can cause torque overshoot and hence increases the torque ripple [5,6]. This is undesirable especially for applications that require precise torque control.

This paper presents a simple torque controller to replace the existing three level hysteresis comparator to give a constant torque switching frequency and reduces the torque ripple. The controller was initially proposed in [7], but a systematic controller design was not given. In this paper, an approximate frequency domain model, which is used as a guide to the controller design, is developed. The simple control structure of the DTC is preserved yet significant improvement is achieved as demonstrated by the simulation and experimental results.

The rest of the paper is organized as follows. Section II described the principle of DTC of IM. Section III proposed the new torque controller and presents its approximate frequency domain model. The frequency domain model is then used as a guide for the PI controller's parameters used in the proposed torque controller. Section IV presents the simulation and experimental results. And finally Section V draws the conclusions.

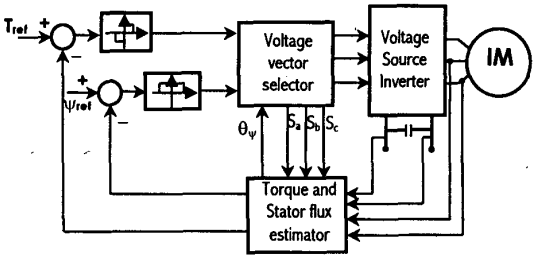

Fig.1 Basic DTC drive configuration

0-7803-6355-8/00/ $10.00 © 2000 IEEE

II. DIRECT TORQUE CONTROL OF INDUCTION MACHINE

The induction machine in general reference frame is represented by the following space vector equations:

$$\bar{v}_s^g = R_s \bar{i}_s^g + \frac{d\bar{\psi}_s^g}{dt} + j\omega_g \bar{\psi}_s^g \quad (1)$$

$$0 = R_r \bar{i}_r^g + \frac{d\bar{\psi}_r^g}{dt} + j(\omega_g - \omega_r)\bar{\psi}_r^g \quad (2)$$

$$\bar{\psi}_s^g = L_s \bar{i}_s^g + L_m \bar{i}_r^g \quad (3)$$

$$\bar{\psi}_r^g = L_r \bar{i}_r^g + L_m \bar{i}_s^g \quad (4)$$

The super-script 'g' in the above equations denotes that the quantity is referred to the general reference frame. The torque and mechanical dynamics of the machine are expressed as:

$$T_e = \frac{3}{2}\frac{p}{2}\bar{\psi}_s^g \times \bar{i}_s^g \quad (5)$$

$$J\frac{d\omega_m}{dt} = J\frac{2}{p}\frac{d\omega_r}{dt} = T_e - T_{load} \quad (6)$$

The voltage vector of the three-phase VSI, with the DC link voltage V_d is given by:

$$\bar{v}_s(t) = \frac{2}{3}V_d\left(S_a(t) + S_b(t)a + S_c(t)a^2\right), \text{ where } a = e^{j\frac{2}{3}\pi} \quad (7)$$

$S_a(t)$, $S_b(t)$ and $S_c(t)$ are the switching functions of each leg of the VSI, which can take a value of either 1 or 0.

In DTC, the eight possible combinations of S_a, S_b and S_c are utilized to satisfy the demand of the stator flux and torque within their hysteresis bands, simultaneously. Table 1 gives the possible combinations of voltage vectors that can be applied at different stator flux sectors defined in Fig. 2. Stator flux error status (or torque error status) of 1 and 0 indicates that the stator flux (or torque) needs to be increased or decreased respectively. When a large negative torque error occurs, such as during reversal or braking, the torque error status becomes –1 and reverse voltage vectors will be selected. The *radial* valtage vectors are avoided to avoid high switching frequency, hence zero voltage vectors are selected when the torque and flux need to be decreased simultaneously.

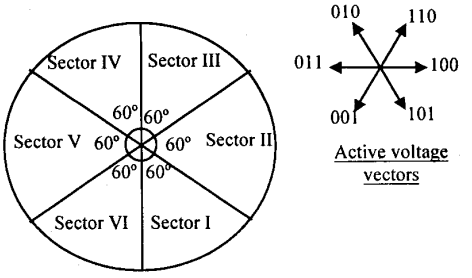

Fig. 2 Six sectors of the stator flux plane

III. PROPOSED TORQUE CONTROLLER

The proposed torque controller consists of two triangular waveform generators, two comparators and a PI controller as shown in Fig. 3 [7]. The two triangular waves (C_{upper} and C_{lower}), are 180° out of phase with each other. The dc offsets for C_{upper} and C_{lower} are set to half of its peak-peak value; the upper dc offset is positive while the lower is negative.

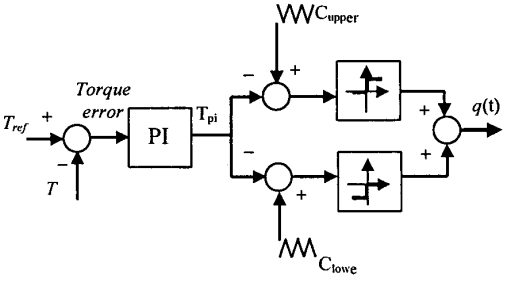

Fig. 3 Proposed torque controller

In principle, the output of the proposed torque controller is similar to that of the three level hysteresis comparator [1], which can be either of three states: –1, 0 or 1. The output, designated by q(t), is given by:

$$q(t) = \begin{cases} 1 & for\ T_{pi} \geq C_{upper} \\ 0 & for\ C_{lower} < T_{pi} < C_{upper} \\ -1 & for\ T_{pi} \leq C_{lower} \end{cases} \quad (8)$$

Table 1 Voltage vectors selection table

STATOR FLUX ERROR STATUS	TORQUE ERROR STATUS	SECTOR I	SECTOR II	SECTOR III	SECTOR IV	SECTOR V	SECTOR VI
1	1	100	110	010	011	001	101
	0	000	111	000	111	000	111
	-1	001	101	100	110	010	011
0	1	110	010	011	001	101	100
	0	111	000	111	000	111	000
	-1	011	001	101	100	110	101

q(t), along with stator flux error status and stator flux position, will be used to determine the appropriate voltage vectors to be selected. The choices of voltage vectors are given by Table 1.

The average value of the output, $\bar{q}(t)$, is defined as continuous duty ratio and is denoted by d(t). The average of q(t) is taken over an interval that equals the period of the triangular carrier waveforms, T_{tri}, which means that d(t) can take a value between −1 and 1.

$$d(t) = \frac{1}{T_{tri}} \int_{t}^{t+T_{tri}} q(t)\, dt \tag{9}$$

A. Modeling of the controller

In this section, the frequency domain model of the torque loop will be developed. It will be used as a guide in the selection of the controller's parameters. In order to simplify the analysis, the following assumptions are made:

(a) In stator flux reference frame, such that the q component of the stator flux is zero, the active voltage vectors are always orthogonal to the stator flux. This means that in this reference frame, the d component of the voltage vectors is zero. i.e., $v_{sd}^{\psi s} = 0$ and $v_{sq}^{\psi s} = \left|\bar{v}_s^{\psi s}\right|$.

(b) In the stator flux reference frame mentioned in (a), the q component of the rotor flux is neglected, i.e. $\psi_{rq}^{\psi s} = 0$ and hence $\psi_{rd}^{\psi s} = \left|\bar{\psi}_r\right|$.

The average equation of the torque needs to be derived first. The positive and negative torque slope equations in d-q terms are given by [8]:

$$\frac{dT_e^+}{dt} = -\frac{T_e}{\sigma\tau_{sr}} + \frac{3}{2}\frac{p}{2}\frac{L_m}{\sigma L_s L_r}\left[-v_{ds}\psi_{qr} + v_{qs}\psi_{dr} - \omega_r \cdot \left(\psi_{ds}\psi_{dr} + \psi_{qs}\psi_{qr}\right)\right] \tag{10a}$$

$$\frac{dT_e^-}{dt} = -\frac{T_e}{\sigma\tau_{sr}} - \frac{3}{2}\frac{p}{2}\frac{L_m}{\sigma L_s L_r}\omega_r\left[\psi_{ds}\psi_{dr} + \psi_{qs}\psi_{qr}\right] \tag{10b}$$

In stator flux reference frame and applying assumptions (a) and (b), equations (10a) and (10b) can be written as:

$$\frac{dT_e^+}{dt} = -\frac{T_e}{\sigma\tau_{sr}} + \frac{3p}{4}\frac{L_m}{\sigma L_s L_r}\left\{v_s^{\psi s}\psi_s - (\omega_r - \omega_{\psi s}) \cdot (\psi_s \psi_r^{\psi s})\right\} \tag{11a}$$

$$\frac{dT_e^-}{dt} = -\frac{T_e}{\sigma\tau_{sr}} - \frac{3p}{4}\frac{L_m}{\sigma L_s L_r}(\omega_r - \omega_{\psi s}) \cdot (\psi_s \psi_r^{\psi s}) \tag{11b}$$

Where $\dfrac{1}{\sigma\tau_{sr}} = \left(\dfrac{1}{\sigma\tau_s} + \dfrac{1}{\sigma\tau_r}\right)$

In normal operation, the stator flux, hence the rotor flux, are kept at their rated value and can be assumed constant. During the positive slope, the instantaneous stator flux frequency is denoted by $\omega_{\psi s}$, whereas during negative slope (i.e. zero voltage vectors is selected), it is assumed zero. Equation (11b) then reduces to:

$$\frac{dT_e^-}{dt} = -\frac{T_e}{\sigma\tau_{sr}} - \frac{3p}{4}\frac{L_m}{\sigma L_s L_r}(\omega_r)\left\{\psi_s \psi_r^{\psi s}\right\} \tag{12}$$

It can be shown that the instantaneous stator flux frequency, $\omega_{\psi s}$, is related to the synchronous frequency, ω_e by:

$$\omega_{\psi s} = \frac{\omega_e}{d} \tag{13}$$

Equation (13) can be written as:

$$\omega_{\psi s} = \frac{\omega_{slip} + \omega_r}{d} \tag{14}$$

Where ω_{slip} is the average slip frequency over one cycle of stator flux. Substituting (13) into (11) and simplifying terms give:

$$\frac{dT_e^+}{dt} = -AT_e + Bv_s^{\psi s} + K_1\left(\frac{\omega_e}{d} - \omega_r\right) \tag{15}$$

$$\frac{dT_e^-}{dt} = -AT_e - K_1\omega_r \tag{16}$$

Where

$$A = \frac{1}{\sigma\tau_{sr}} \qquad B = \frac{3p}{4}\frac{L_m}{\sigma L_s L_r}\psi_s$$

$$K_1 = \frac{3p}{4}\frac{L_m}{\sigma L_s L_r}(\psi_s \psi_r^{\psi s})$$

Equations (15) and (16) are averaged to give:

$$\frac{dT_e}{dt} = -AT_e + Bv_s^{\psi s}d + K_1\left(\omega_e - \omega_r\right) \tag{17}$$

or

$$\frac{dT_e}{dt} = -AT_e + Bv_s^{\psi s}d + K_1\left(\omega_{slip}\right) \tag{18}$$

To linearise (18) around an operating point, small perturbations designated by "~" are introduced in T_e, d and

ω_{slip} – the DC link voltage is assumed constant hence no perturbation is introduced in $v_s^{\psi s}$. Equation (18) becomes:

$$\frac{dT_e}{dt} + \frac{d\tilde{T}_e}{dt} = -A(T_e + \tilde{T}_e) + Bv_s^{\psi s}(d + \tilde{d}) + K_1(\omega_{slip} + \tilde{\omega}_{slip}) \tag{19}$$

To obtain a steady state equation, all the purturbations (and its derivative) and $\frac{d\tilde{T}_e}{dt}$ are set to zero. Thus, the steady state equation is :

$$0 = -AT_e + Bv_s^{\psi s} d + K_1 \omega_{slip} \tag{20}$$

The equation for the small perturbation components is given by:

$$\frac{d\tilde{T}_e}{dt} = -A\tilde{T}_e + Bv_s^{\psi s}\tilde{d} + K_1\tilde{\omega}_{slip} \tag{21}$$

Taking the Laplace transform of (21), the torque T_e(s) can be written as:

$$T_e(s) = \frac{Bv_s^{\psi s} d(s) + K_1 \omega_{slip}(s)}{s + A} \tag{22}$$

B. PI controller design

Setting the slip frequency, ω_{slip}, to zero, the block diagram of the frequency domain model of the torque loop with the PI controller is as shown in Fig. 4. The transfer function between T_{pi} and d(t) is linear and can be shown equal to $1/C_{p\text{-}p}$. This relation is linear as long as T_{pi} does not exceed the peak to peak value of the triangular carrier ($C_{p\text{-}p}$). During start-up or speed reversing this is however not true, hence the frequency domain model has to include the saturation block to limit d(s) between –1 and 1. The PI controller transfer function is given by:

$$\text{PI controller}: K_p \frac{\left(s + K_i/K_p\right)}{s} \tag{23}$$

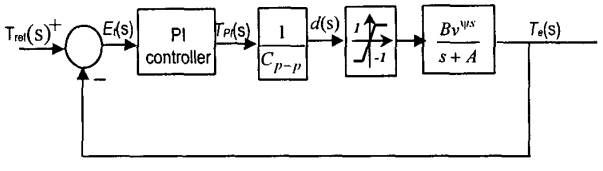

Fig. 4 Block diagram of the torque-loop in frequency domain

For the torque controller to function properly, the slope of T_{pi} must be ensured not to exceed the triangular carrier slope, which is mainly determined by the proportional gain, K_p. Thus, for the positive slope, from (15),

$$\langle ASC \rangle \geq \left\{ -AT + BV_s^{\psi s} + K_1\left(\frac{\omega_e}{d} - \omega_r\right)\right\} K_p^+ \tag{24}$$

Where ASC is the Absolute Slope of the Carrier. For the negative slope, from (16), the following must be satisfied:

$$\langle ASC \rangle \geq \left| -AT - K_1\omega_r \right| K_p^- \tag{25}$$

For the positive slope, the minimum K_p^+ is assumed to occur when $\omega_r = 0$. While for the negative slope, the minimum K_p^- is assumed when the rotor is at its maximum speed. The value of d used in calculating K_p is obtained from (20). Of the two cases above, the worst case, i.e. the smallest value of K_p, will be chosen.The model becomes less accurate as the frequency approaches one half of the carrier frequency; thus the loop gain crossover frequency should be made smaller than this. If the zero of the PI controller is chosen to be the same as the system pole (i.e. -A), then, K_i is given by:

$$K_i = K_p * A \tag{26}$$

IV. Simulation and Experimental Results

To verify the effectiveness of the proposed torque controller, simulations and experiments on the DTC induction motor drive were carried out. The simulations were conducted using Matlab/SIMULINK simulation package, while the implementation was carried out using a dSPACE DS1102 controller board centered around TMS320C31 digital signal processor. A standard induction motor rated at ¼ hp, 240V, 50Hz is used with a DC generator coupled as a load. The carrier frequency ($1/T_{tri}$) is set to 2.27 kHz for both the simulation and experimental. To minimize the sampling period, the voltage vectors selection table, blanking time of the VSI and protections were implemented using the XC4005E Xilinx FPGA. The experimental set-up is shown in Fig 5. Based on the actual machine parameters (as given in the appendix), and on the steps outlined in the previous section, the PI controller's parameters are calculated as:

$$K_p = 329.9 \text{ and } K_i = 112825.8$$

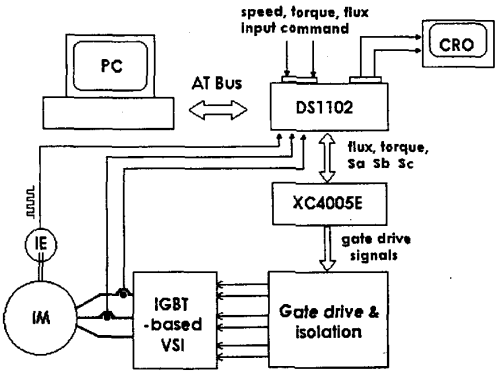

Fig. 5 Experimental set-up

A. Response to a step change in torque reference

A step change in torque reference from 0 to 0.6 N-m is applied to the DTC drive. The simulation result of the torque response is shown in Fig 6a. The corresponding experimental result is shown in Fig. 6b. From the figure, it can be seen that the torque rise time is very short, of about 2-3 ms. The results shows that the simulation and experimental results are in close agreement. Due to relatively smaller torque-loop bandwidth, which is limited by the triangular carrier frequency, the stator flux ripple is reflected in the torque response.

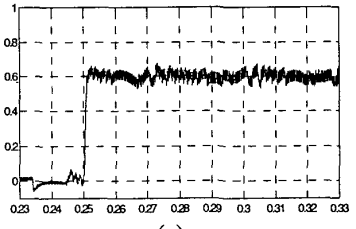

(a)

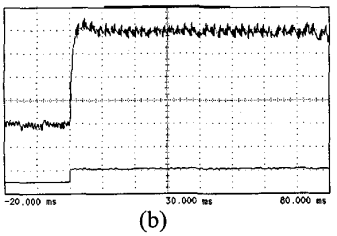

(b)

Fig. 6 Response to step change in torque reference. (a) Simulation (b) Experimental at 0.15 N-m/div

B. Switching Frequency and torque ripple

To look at the effectiveness of the proposed torque controller in maintaining a constant torque switching fequency, a comparision to the conventional hysteresis torque comparator is made. Table 1 gives the calculated device switching frequency from the experiment of the proposed controller and hysteresis based comparators with $\Delta T = 0.06$ N-m and $\Delta T = 0.12$ N-m. The torque switching frequency of the proposed torque controller is fixed at the triangular carrier frequency of 2.27 kH. Since under steady state, the device actively switches in two out of six sectors, the device switching frequency contributed by the torque switching is 1/3 of 2.72kH = 757 Hz. The switching frequency of the proposed controller increases linearly with speed due to the switching contributed by the stator flux hysteresis comparator. The torque hysteresis comparator based controller exhibit wider switching frequency variations. The high switching frequency for the $\Delta T = 0.06$ N-m at low speed is due to the torque overshoot which exceeds the upper torque hysteresis band thus causing the selection of reverse votage vectors to reduce the torque. This in turn resulted in a rapid torque reduction and hence high switching frequency.

The experimental results for steady state torque responses at 10 rad/s and 70 rad/s for the proposed torque controller and the hysteresis based comparator ($\Delta T = 0.12$ N-m) are shown in Fig. 7 and 8 respectively. The torque switching frequency (f_T) as can be observed from Fig. 7, is maintained at about 2.27 kHz, i.e. the frequency of the triangular carrier. For the hysteresis based comparator of Fig. 8, the torque switching frequency varies from 552 Hz at $\omega_r = 10$ rad/s to 1.497 kHz at $\omega_r = 70$ rad/s.

Table 1 Switching frequency at different rotor speed

Rotor speed, ω_r (rad/s)	Switching frequency of the proposed controller (Hz)	Switching frequency of the hysteresis controller with $\Delta T = 0.06$ N-m (Hz)	Switching frequency for hysteresis controller with $\Delta T = 0.12$ N-m (Hz)
10	760	1380	255
30	810	1350	390
50	825	1200	540
70	840	1020	585
Δf_{dv}	80 Hz	360 Hz	330 Hz

Fig. 9 shows the waveforms of the simulation and experimental results of the T_e, C_{upper}, C_{lower}, T_{pi} of the proposed controller, together with the T_e and $q(t)$ of the hysteresis based comparators (ΔT=0.06 and 0.12 N-m) at the rotor speed of 10 rad/s. It can be observed from the figure that the proposed controller managed to reduce the torque ripple significantly. Although the torque hysteresis band for the hysteresis comparator is reduced to 0.06 N-m, the torque ripple is still large due to the applications of reverse voltage vectors (correspond to $q(t) = -1$).

V. Conclusions

The paper has presented a new torque controller to replace the conventional three level hysteresis comparator for the

DTC of induction machine. The design of the controller with the help of an approximate frequency domain model has been presented. The simulations and experimental results of the proposed controller were given. It is shown that with the proposed controller, the torque ripple at low speed is reduced and the torque switching frequency is fixed regardless of the rotor speed.

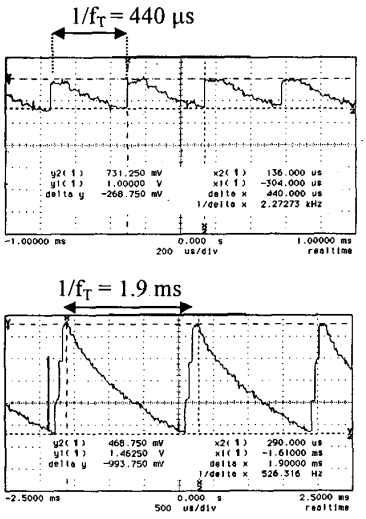

Fig. 7 Torque waveform at ω_r = 10 rad/s. (a) Proposed controller, (b) hysteresis controller

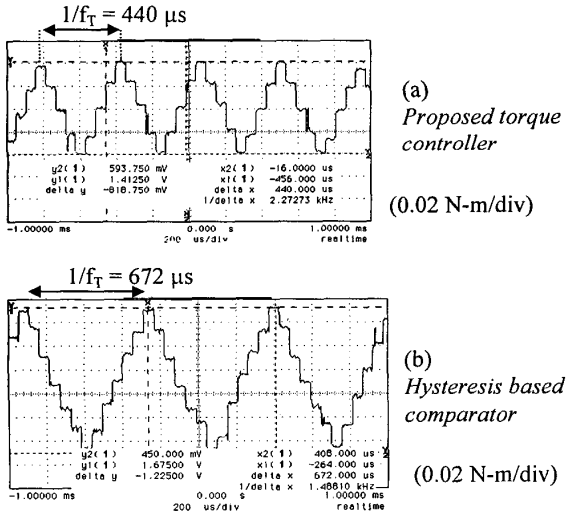

Fig. 8 Torque waveform at ω_r = 70 rad/s. (a) Proposed controller, (b) hysteresis controller

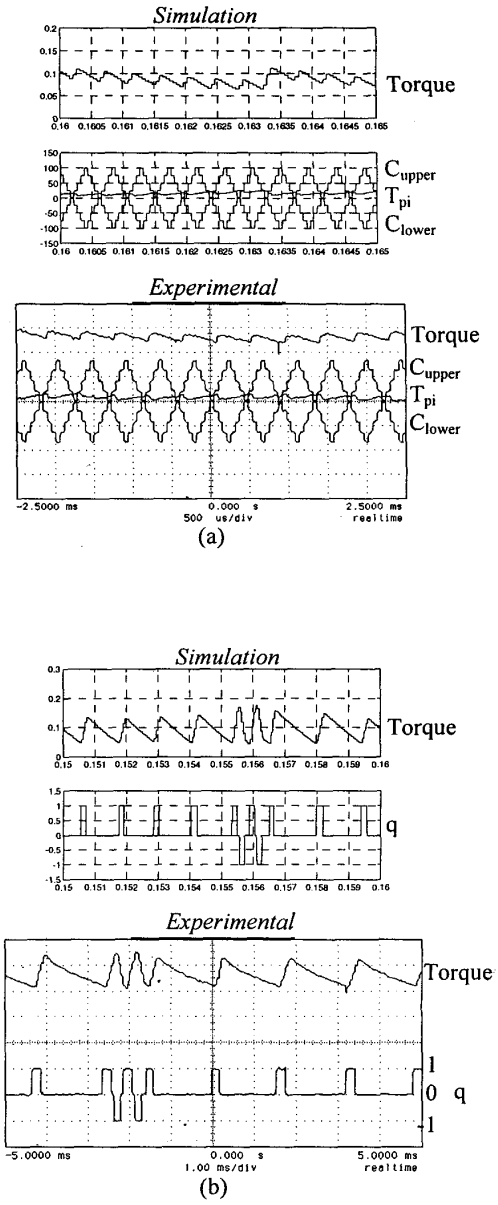

Fig. 9 Simulation and experimental results of the steady state torque at rotor speed of 10 rad/s. Experimental vertical scale: 0.1 N-m/div (a) proposed torque controller, (b) hysteresis based comparator with ΔT = 0.12 N-m, (c) hysteresis based comparator with ΔT = 0.06 N-m.

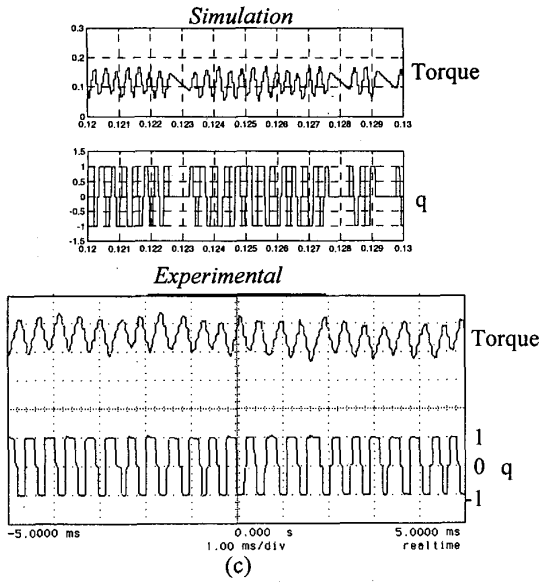

(c)

Fig. 9 (continued)

APPENDIX

Machine parameter

50 Hz, 240V, 2880 rpm, ¼ hp, standard motor

$L_s = 0.6033H$ $R_s = 10.9\ \Omega$

$L_r = 0.6033H$ $R_r = 11.287\ \Omega$

$L_m = 0.6289$

REFERENCES

[1] I. Takahashi.and T. Noguchi "A new quick-response and high-effieciency control strategy of an induction motor", *IEEE Trans. Ind. Appl.*, Vol. IA-22, No 5., 1986.

[2] Y. Li., J. Shao and B. Si "Direct torque control of induction motors for low speed drives considering discrete effect of control and dead-time timing of inverters", *in Conf. Rec. IEEE-IAS Annual meeting*, pp. 781-788., 1997

[3] J.K. Kang and S.K. Sul "Torque ripple minimisation strategy for direct torque control of induction motor", *in Conf. Rec. IEEE-IAS Annual meeting*, pp. 438-443, 1998.

[4] D. Casadei and G. Serra "Analytical investigation of torque and flux ripple in DTC schemes for induction motors", *in Proc. IEEE-IECON'97*, pp. 552-556.,1997

[5] A. Purcell and P. Acarnly "Device switching scheme for direct torque control", *Electronics Letters*, Vol. 34, No.4, pp. 412-414, 1998.

[6] D. Casadei, G. Grandi, G. Serra and A. Tani, "Switching Strategies in direct torque control of induction machine", *International Conf on Electrical Machines*, Paris, France, 1994.

[7] N.R.N. Idris and A.H.M. Yatim,"Reduced torque ripple and constant torque switching strategy for direct torque control induction machines", *APEC 2000*, New Orleans, USA, Feb 2000.

[8] Casadei, D. and Serra, G., "Analytical investigation of torque and flux ripple in DTC schemes for induction motors", *in Proc. IEEE-IECON'97*, pp. 552-556, 1997.